Synthesis and Characterization of)CeO(x-) CuO(1-x Nanocomposite by Simple Aqueous Route for Solar Cell Application

Wafaa M. Salih
Mustansiriyah University
Ahmed Mahdi Rheima (arahema@uowasit.edu.iq)
University of Wasit https://orcid.org/0000-0003-3533-3393
Haider A. Kadhum
Mustansiriyah University

Research Article

Keywords: CeO-CuO nanocomposite, nanoparticles, solar cell, one-pot preparation method

Posted Date: March 16th, 2021

DOI: https://doi.org/10.21203/rs.3.rs-292933/v1

Abstract

This work concludes the synthesis of CeO-CuO nanocomposite by one-pot preparation method using three different molar ratios. The resulted nanocomposite was characterized using UV-Vis, XRD, SEM, EDX and TEM and the results show that this nanocomposite was found as spherical-like nanoparticles with high purity and the average particle size is in the range of 10-20 nm.. Furthermore, this nanocomposite was used in the solar cell application as photo anode and the results showed that the efficiency increase with increase of (x) content in the $(CuO)x–(CeO_2)1\text{-}x$.

1. Introduction

In addition to specifying the comprehensive applications of binary metallic oxide powders or films like $ZnO\text{-}CeO_2$, $CeO_2\text{-}TiO_2$ and NiCuO2, the design and synthesis have recently continued to attract interest from both academia and industry [1-8]. A mixture comprising two stages with a different chemical composition is part of the binary material analysis. From both realistic and fundamental viewpoints, this has received a lot of attention. The combination of the physical properties of such materials will lead to the creation of the desired response material. The magnetic or optical features can be different if the particle size is reduced to very small dimensions. The interest in the binary oxide region has grown considerably. Binary materials are of outstanding quality including high melting points, high hardness, low temperature coefficients, low density, high stability of chemicals, high thermal conductivity, high expansion, as well as better mechanical qualities such as increasing resistance to wear, high specific resistance and special modulus. [9-15]. The intense interactions between the binary oxide systems and intimately packaged nanoparticles on the surface are widely recognized as not just an easy overlap of the properties of the individual components with the characteristics of the binary materials obtained. The goal of the synthesis of multi-component materials was therefore to combine the developments of different stages so that their applications could be improved and further extended. A type of metal oxide semiconductor is copper oxide (CuO), that is narrow energy gap (1.2 eV) [16]. Due to its broad use in gas sensors and as a catalyst and optoelectronic components [17,18], A lot of attention has been drawn. Cerium oxide of rare earth (CeO2) is an n-type metal semiconductor with a wide band gap (3.0-3.2 eV) [19] and a wide band gap. In other areas, as catalysts, ultraviolet filters and mechanical and chemical polishing there are also various applications [20,21]. In different new applications of the material sciences, a mixture of p-type and n-type metal oxide semiconductors may be used. $CuO\text{-}TiO_2$, $SnO_2\text{-}NiO$ and $CuO\text{-}SnO_2$ can be prepared in different presses for the various forms of composite semiconductor oxides. As CuO-CeO2 is more commonly used in catalysis, water gas shifts and solid oxide-powered cell (SOFC)[22], the semiconductor binary oxide nanomaterials have become very interested. Binary metal oxide nanomaterials will typically boost these functions in comparison with their elements. In order to create a compound which has the ideal properties, the researchers have defined and developed CuO-CeO2 with various structural features, in order to make the combined benefits of two compounds. To synthesize $CuO\text{-}CeO_2$ nanomaterial, various techniques such as sono-chemical, hydrothermal, mechano-chemical and solvo-thermal methods have been used [23-25]. However, due to the related complex procedures,

most of these approaches present difficulties with their use in industrial development, leading to many reaction conditions like severe reaction conditions.

Another downside to the technologies is the toxic by-product/toxic reagent that release during the synthesis process. New aspect of the current research is that the approach can have many benefits over the above approaches, some of which are briefly summarized: the production can be achieved without any harmful pollutants, highly adaptable and easy to use in many high-purity applications.

2. Experimental Work

2.1 Materials

Cerium nitrate $Ce(NO_3)_2.6H_2O$ (99%) and Copper nitrate $Cu(NO_3)_2.3H_2O$ (99%) were used as a precursors materials without any purification steps, purchased from Sigma-Aldrich. The following materials were purchase from Fluka; sodium hydroxide and ammonia to complete the reaction in addition to the stabilizer, urea was used to simplify the dispersal of nanoparticles.

2.2 Methods

2.2.1. Preparation of binary metal oxides

Different molar ratios from cerium nitrate and copper nitrate (0.25, 0.5, 0.75) were dissolved in 40 ml of deionized water separately then sodium hydroxide was added drop by drop to copper nitrate under stirring at $50C^o$ with 1:2 ratio and ammonia was dropped to cerium nitrate under 1200 rpm stirrer speed. After that 5 g from urea was dissolved in 50 ml of de-ionized water and added to the mixture solutions under stirring at $60C^o$ until blush brown suspension was formed. The mixture of metals oxide washed two times for distilled water and ethanol then the powder was separated by centrifuge, then dried in the oven at 90 C^o for 5h. The mixture was calcinated at $400C^o$ for half an hour to get dark brown color product.

2.2.2. Fabricated solar cell

Two types of substrate were used in this research to fabricate solar cell:

1. ITO glass (indium tin oxide) cutted into 2*2 cm^2 clean firstly in sonicator for 15 minutes with deionized water, then used ethanol purity 99% in sonicated for 10 minutes
2. Single crystal Si P-type wafer, the thickness 300 μm with an (100) orientation and resistivity ~0.4 (Ω. Cm). The wafer cut into 2*2 cm^2, chemical etching was done to get rid from impurities, immerse the pieces of silicon wafer in HF acid concentration 10% for 5 minutes, after that clean with distilled water and ethanol then dry with blower.

To produce (CuO)x–(CeO_2)1-x photo anode, drop cast technique used deposited thin films of this binary metallic oxide on substrate by used Blade method. 0.1 g (CuO)x-(CeO_2)1-x powder was mixed with 5 ml of absolute ethanol under ultrasonic for 3 minutes in order to obtain thick solution nanoparticles. The resulted thick solution was applied on a conductive side of ITO glass, then heated the samples at 100^o for an hour to ensure good adhesion the binary metallic oxide nanoparticles with the substrate while heated at 200^o for two hours for samples with silicon wafer substrate. When deposited (CuO)x–(CeO_2)1-x powder nano particles by spin coating technique [26].

For the purpose of electrical connection with other devices, Al electrode as a back contact curried out using thermal evaporation coating unit Edward (model E306A) evacuated of 6*10 $^{-5}$ Torr, aluminum foil with purity 99% put in tungsten boat done at room temperature with thickness a round 300 nm.

The J-V curve of the sun simulator was calculated under AM1.5 illumination (100 W/cm^2) provided by halogen lamps and 25 C^o solar cell temperature using D.C. power supply, Keithly digital electrometer 616 and voltmeter. The height of the lamps was matched with the short-circuit current of the calibration sample were as limits at (20 cm).

3. Results And Discussion

3.1. X-ray Diffraction

Figure 2 reveals x- ray diffraction patterns at different ratio concentration of $(CuO)_x–(CeO_2)_{1-x}$ where x= (0.25 Figure 1 (a), 0.5 Figure 1 (b) and 0.75 Figure 1 (c)), diffraction peaks confirm the presence of CeO_2 and CuO nanoparticles with cubic and monoclinic system, respectively. Miller indices for all CuO diffraction peak associated to (110), (002), (111), (200), (021) and (220) which found at 2Θ= 32.8, 35.2, 38.6, 46.54, 56.51 and 68.5^o [27] while the diffraction peaks related of CeO are (111), (200), (220), (311), (400) and (331) which found at 2Θ=28.8, 33.35, 47.65, 56.34, 69.41 and 76.54^o [28].

The cubic and monoclinic structures were found in binary metal oxide NPs powder of CeO_2 and CuO were found to be satisfied Patterns of standard diffraction card of CeO_2 (JCPDS card No. 34-0394) and CuO (JCPDS card No. 48-1548) within the same synthesis binary $(CuO)_x–(CeO_2)_{1-x}$ nanoparticles, CuO and CeO_2 nanoparticles where formed, it could be inferred. In a single sample the effect of the location of the peaks on one another might probably be preserved in two phases.

Table 1 summarized the crystallized size value of different concentration for binary metallic samples, notice from the table decreasing the crystalized size value with increasing copper oxide concentration which be 15.4, 13.5 and 9.4 nm at x=0.25, 0.5 and 0.75 respectively.

Table (1) Crystal size, FWHM, 2Θ, Micro strain and dislocation density

Ratio concentration (x)	Average crystalized size (nm)	Crystallite size for highest peak (nm)	FWHM (degree)	2Θ	d-spacing (A^o)	Strain (10^{-4})	Dislocation density(10^{-3}) (line/nm^2)
0.25	15.4	10.96	0.7872	28.3951	3.143	67.2	8.3
0.5	20	14.5	0.5904	28.3327	3.150	50.9	4.7
0.75	9.4	9	0.9840	28.6331	3.117	83.9	12.34

3.2. UV- Visible characteristic:

Optical absorbance and transmittance measurement were conducted for all samples in order to evaluate the optical band gap of the synthesized binary metallic nanoparticles using tauce eqn.

Figures 2(a-c) represent an optical absorption spectra as a function of a wavelength for $(CuO)_x-(CeO_2)_{1-x}$, the results show the absorbance spectrum increase above 300 nm for all specimen and this agree with absorbance characteristic of UV –Visible range of copper oxide and cerium oxide semiconductors .

Additionally, the discrepancy in ionic radius of Ce and Cu conducting to lattice distortion when Ce^{+2} ion replaced Cu^{+2} ions and third induced to reduce of the energy band gap values when the concentration ratio x increase, Figures 2(d-f) show the energy gap values estimated by plotted $(\alpha\ hv)^n$ versus photon energy (hv), where n=2 for direct allowed transition because all samples of copper oxide and cerium oxide obey to the rule of direct optical transition.

Table 2. The energy gap value for all specimen ($CuO-CeO_2$) nanoparticles where noted to be (3.2 ev), (2.5 eV) and (2 eV) when x = 0.25 , 0.5 and 0.75 respectively.

ratio concentration (x)	Energy gap (eV)
0.25	3.2
0.5	2.5
0.75	2

3.3. FESEM and EDX Analysis

Figure 3(a-c) showed the FESEM images of the synthesis binary oxide nanoparticles ((CuO)x–(CeO_2)1-x) at various concentration (x= 0.25, 0.5 and 0.75), it is evident from those images spherical and regular shape of nanoparticles were formed, also the increasing in x value contribute to increasing of surface area to a value which leads to improvement the properties like efficiency of solar cell. For Figure 3(a-c) at x= 0.25, 0.5 and 0.75 respectively, clearly show the average grain size is in the range of 10-20 nm.

The basic composition of the synthesis nanoparticles prepared at various concentrations was analyzed using the EDX technique. The spectrum and atomic composition of the sample of the nanoparticles are showing. Table 3 show the theoretical and practical values of this composition it is clear from the table conformity in theoretical with practical values and no sign of other elements in the spectra were observed. In order to further affirm the homogeneity of the material of the NPs were analyzed by EDAX in mapping mode with synthesized nanoparticles whose information is summarized in Figure 4. This analysis firmly supports the findings of Figure 3, provides dependent mapping mode ((CuO_x)-$(CeO_2)_{1-x}$) representations.

Table 3. Theoretical and practical EDX data

Metal-Oxygen	Practical EDX			Theoretical EDX		
Cu:Ce:2O	Cu	Ce	O	Cu	Ce	O
0.25:0.75:1	10.96	72.7	15.33	10.3	68.8	20.9
0.5:0.5:1	18.61	67.15	14.24	25.28	55.67	19.07
0.75:0.25:1	35.48	43.44	21.08	46.41	34.11	19.48

3.4. TEM analysis

TEM images in Figure 5 clearer the homogeneous morphology of the metallic binary oxides synthesized $(CuO)_x - (CeO_2)_{1-x}$ nanoparticles ,for this nanocomposite TEM results clearly show the binary –content nanocomposite (CeO-CuO), i.e clarify the existence of all reaction materials ,the efficient reactions between these two materials and the stable grafting of the prepared nanocomposite material are good evidence of this assignment .The results are clear to be in good agreement with crystal size ranging from (10-20) nm at x=(0.25-0.75), respectively.

3.5. J-V Characteristic

The J-V properties of (CuO)x–(CeO2)1-x under lighting display a high value at a given voltage which shows that the light absorption by the active binary oxide layer produces photo curricular contributions by a supplementary output at the barrier into free-of-charge transmitters, i.e. the (CuO) x- (CeO2)1-x interface. The free electrons and holes were accelerated towards the electrodes under the influence of the electric field at the junction, and crossed the potential barrier at the interface. Fig. (8) and (9) show the J-V characteristic for different types of electrode (ITO, P-Si) and various ratio concentration (x=0.25,0.5,0.75), where current density decreased exponentially with voltage. For all samples, it is obvious that efficiency increase with increase of (x) content for ITO substrate solar cell be (6.48,7.68 and 9.6 %) at (x= 0.25,0.5 and 0.75) respectively ,this indicator that increase of (x) content lead to increase in surface area to volume because Copper oxide have smallest particle size than Cerium oxide firstly and energy gap at x=0.75 have smallest value Eg=1.9Ev, While efficiency become (14.52%) at (x=0.75 for P-Si substrate as a result for high matching Si substrate with binary metallic oxide .By using (3) and (4) equation, J-V

parameters (Imax, Vmax, Isc, Voc, and F.F) were calculated and list of in table ().It is show from the table that Ics and Voc change in a non-systematic sequence with x content for the two substrate (ITO, P-Si), i.e decrease and increase with the increase of (x) content

$$\eta = \frac{Pm}{Pin} \quad 100\%$$

$$\eta = \frac{F.F\ IscVoc}{Pin} * 100\% \qquad \ldots\ldots (3)$$

$$F.F = \frac{ImVm}{IscVoc} \qquad \ldots\ldots\ldots (4)$$

Pm = maximum power can be generated by the device, Pin = the incident power equal to (100 W / cm^2), Im = maximum current (mA), Vm = maximum voltage(V), Voc =Open circuit voltage (V), Isc = Short circuit current (mA) and F.F = fill factor.

Conclusions

This work concludes that different molar ratios from cerium nitrate and copper nitrate (0.25, 0.5, 0.75) results in $(CuO)_x$–$(CeO_2)_{1-x}$ which characterized using different techniques of nanomaterials. The results show that this nano bimetallic oxide composites are found as spherical-like nano material with very small grain size (10-20) nm.

The results of solar cell proved that these nano bimetallic composites are able to be used in solar cell applications.

References

1. Muñoz-Chilito, J. F., & Rodríguez-Páez, J. E. (2021). ZnO-CeO2 nanocomposites: Synthesis, characterization and evaluation of their action on polluting gases emitted by motorcycles. *Journal of Environmental Chemical Engineering*, *9*(1), 104890.
2. Liao, M., Guo, C., Guo, W., Hu, T., Xie, J., Gao, P., & Xiao, H. (2021). One-step growth of CuO/ZnO/CeO2/ZrO2 nanoflowers catalyst by hydrothermal method on Al2O3 support for methanol steam reforming in a microreactor. *International Journal of Hydrogen Energy*.
3. Qian, J., Wang, Y., Pan, J., Chen, Z., Wang, C., Chen, J., & Wu, Z. (2020). Non-enzymatic glucose sensor based on ZnO–CeO2 whiskers. *Materials Chemistry and Physics*, *239*, 122051.
4. Sui, L., Yu, T., Zhao, D., Cheng, X., Zhang, X., Wang, P., ... & Huo, L. (2020). In situ deposited hierarchical CuO/NiO nanowall arrays film sensor with enhanced gas sensing performance to H2S. *Journal of hazardous materials*, *385*, 121570.
5. Ramu, A. G., Kumari, M. A., Elshikh, M. S., Alkhamis, H. H., Alrefaei, A. F., & Choi, D. (2021). A facile and green synthesis of CuO/NiO nanoparticles and their removal activity of toxic nitro compounds in aqueous medium. *Chemosphere*, 129475.

6. Zeng, Y., Wang, Y., Hongmanorom, P., Wang, Z., Zhang, S., Chen, J., ... & Kawi, S. (2021). Active sites adjustable phosphorus promoted CeO2/TiO2 catalysts for selective catalytic reduction of NOx by NH3. *Chemical Engineering Journal*, *409*, 128242.
7. Nimmas, T., Wongsakulphasatch, S., Cheng, C. K., & Assabumrungrat, S. (2020). Bi-metallic CuO-NiO based multifunctional material for hydrogen production from sorption-enhanced chemical looping autothermal reforming of ethanol. *Chemical Engineering Journal*, *398*, 125543.
8. Yu, H., Qian, C., Ren, H., Chen, M., Tang, D., Wu, H., & Lv, R. (2020). Enhanced catalytic properties of bimetallic sulfides with the assistance of graphene oxide for accelerating triiodide reduction in dye-sensitized solar cells. *Solar Energy*, *207*, 1037-1044.
9. Guo, S., Zhang, Y., Ge, Y., Zhang, S., Zeng, H., & Zhang, H. (2019). 2D V-V Binary materials: status and challenges.*Advanced Materials*, *31*(39), 1902352.
10. Shibata, K., Kiyoura, T., Kitagawa, J., Sumiyoshi, T., & Tanabe, K. (1973). Acidic properties of binary metal oxides. *Bulletin of the Chemical Society of Japan*, *46*(10), 2985-2988.
11. Ao, B. (2021). Scaling the existence state of hydrogen in metal binary oxides. *Acta Materialia*, *203*, 116463.
12. Abu-Dief, A. M., Essawy, A. A., Diab, A. K., & Mohamed, W. S. (2021). Facile synthesis and characterization of novel Gd2O3–CdO binary mixed oxide nanocomposites of highly photocatalytic activity for wastewater remediation under solar illumination. *Journal of Physics and Chemistry of Solids*, *148*, 109666.
13. Li, G., Li, N., Sun, Y., Qu, Y., Jiang, Z., Zhao, Z., ... & Hao, Z. (2021). Efficient defect engineering in Co-Mn binary oxides for low-temperature propane oxidation. *Applied Catalysis B: Environmental*, *282*, 119512.
14. Pan, W. G., Zhou, Y., Guo, R. T., Zhen, W. L., Hong, J. N., Xu, H. J., ... & Guo, S. Y. (2014). Influence of calcination temperature on CeO2-CuO catalyst for the selective catalytic reduction of NO with NH3.*Environmental Progress & Sustainable Energy*, *33*(2), 385-389.
15. Cam, T. S., Petrova, A. E., Ugolkov, V. L., Sladkovskiy, D. A., & Popkov, V. I. (2020). On the SCS Approach to the CeO 2/CuO Nanocomposite: Thermochemical Aspects and Catalytic Activity in n-Hexane Conversion. *Russian Journal of Inorganic Chemistry*, *65*, 725-732.
16. Radhakrishnan, A. A., & Beena, B. B. (2014). Structural and optical absorption analysis of CuO nanoparticles. *Indian Journal of Advances in Chemical Science*, *2*(2), 158-161.
17. Steinhauer, S., Brunet, E., Maier, T., Mutinati, G. C., Köck, A., Freudenberg, O., ... & Resel, R. (2013). Gas sensing properties of novel CuO nanowire devices. *Sensors and Actuators B: Chemical*, *187*, 50-57.
18. Alves, D., Santos, C. G., Paixão, M. W., Soares, L. C., de Souza, D., Rodrigues, O. E., & Braga, A. L. (2009). CuO nanoparticles: an efficient and recyclable catalyst for cross-coupling reactions of organic diselenides with aryl boronic acids. *Tetrahedron Letters*, *50*(48), 6635-6638.
19. Chen, F., Ho, P., Ran, R., Chen, W., Si, Z., Wu, X., ... & Lee, C. (2017). Synergistic effect of CeO2 modified TiO2 photocatalyst on the enhancement of visible light photocatalytic performance. *Journal of Alloys and Compounds*, *714*, 560-566.

20. Hoshino, T., Kurata, Y., Terasaki, Y., & Susa, K. (2001). Mechanism of polishing of SiO2 films by CeO2 particles. *Journal of Non-Crystalline Solids*, *283*(1-3), 129-136.
21. Cassee, F. R., Van Balen, E. C., Singh, C., Green, D., Muijser, H., Weinstein, J., & Dreher, K. (2011). Exposure, health and ecological effects review of engineered nanoscale cerium and cerium oxide associated with its use as a fuel additive. *Critical reviews in toxicology*, *41*(3), 213-229.
22. Prasad, R., & Rattan, G. (2010). Preparation methods and applications of CuO-CeO2 catalysts: A short review. *Bulletin of Chemical Reaction Engineering & Catalysis*, *5*(1), 7.
23. Borchers, C., Martin, M. L., Vorobjeva, G. A., Morozova, O. S., Firsova, A. A., Leonov, A. V., ... & Cholakh, S. O. (2019). CuO-CeO2 nanocomposite catalysts produced by mechanochemical synthesis. *AIP Advances*, *9*(6), 065115.
24. Chen, T. W., Chinnapaiyan, S., Chen, S. M., Ali, M. A., Elshikh, M. S., & Mahmoud, A. H. (2020). A feasible sonochemical approach to synthesize CuO@ CeO2 nanomaterial and their enhanced non-enzymatic sensor performance towards neurotransmitter. *Ultrasonics sonochemistry*, *63*, 104903.
25. Liu, Y., Mao, D., Yu, J., Zheng, Y., & Guo, X. (2020). Facile preparation of highly active and stable CuO–CeO 2 catalysts for low-temperature CO oxidation via a direct solvothermal method. Catalysis Science & Technology, 10(24), 8383-8395.
26. Huang, J., Li, G., & Yang, Y. (2008). A semi-transparent plastic solar cell fabricated by a lamination process.*Advanced materials*, *20*(3), 415-419.
27. Xu, J. F., Ji, W., Shen, Z. X., Tang, S. H., Ye, X. R., Jia, D. Z., & Xin, X. Q. (1999). Preparation and characterization of CuO nanocrystals. *Journal of Solid State Chemistry*, *147*(2), 516-519.
28. Bera, P., & Anandan, C. (2014). XRD and XPS studies of room temperature spontaneous interfacial reaction of CeO 2 thin films on Si and Si 3 N 4 substrates. *RSC Advances*, *4*(108), 62935-62939.

Figures

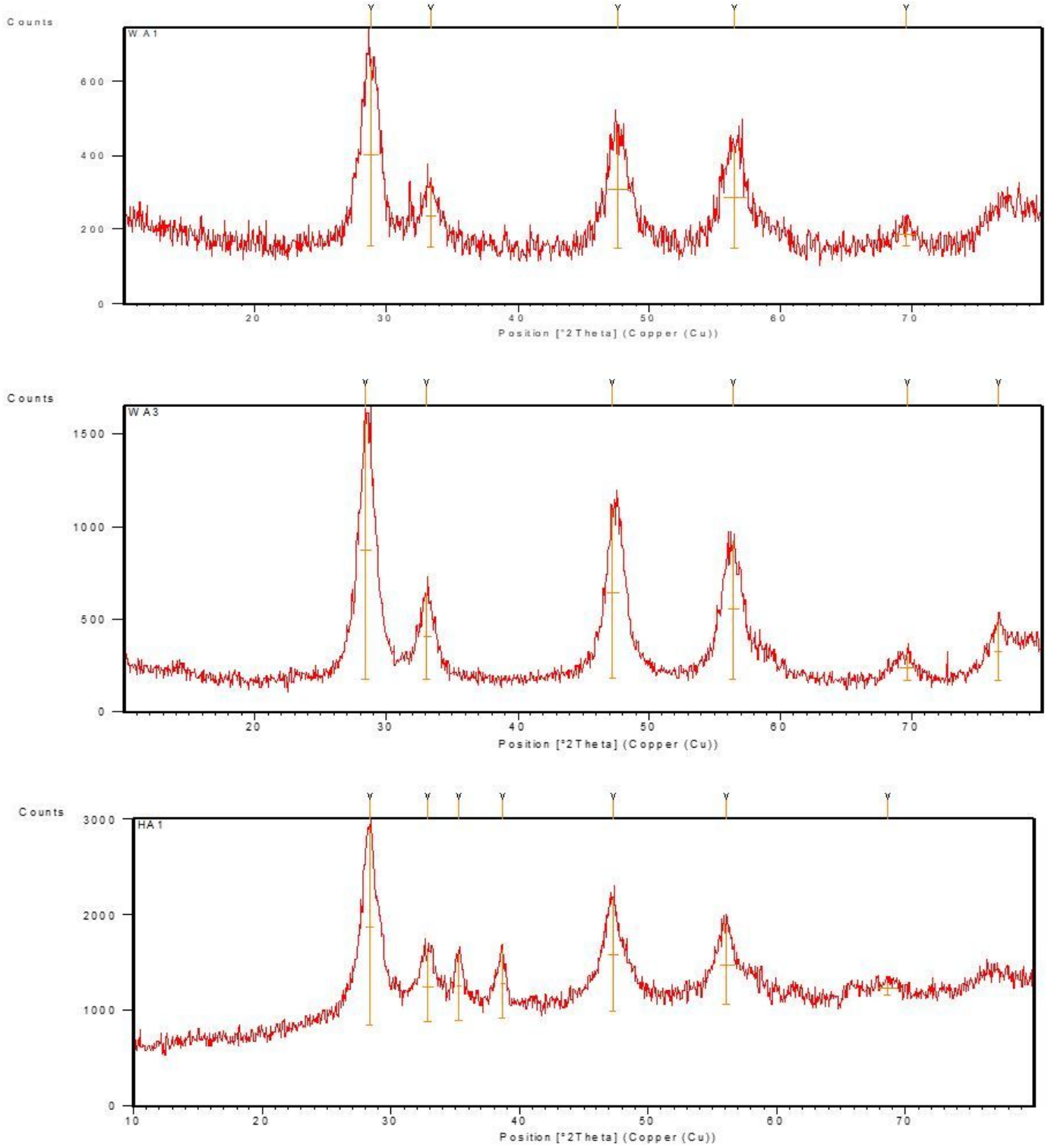

Figure 1

XRD of (a), 0.25, (b) 0.5 and (c) 0.75

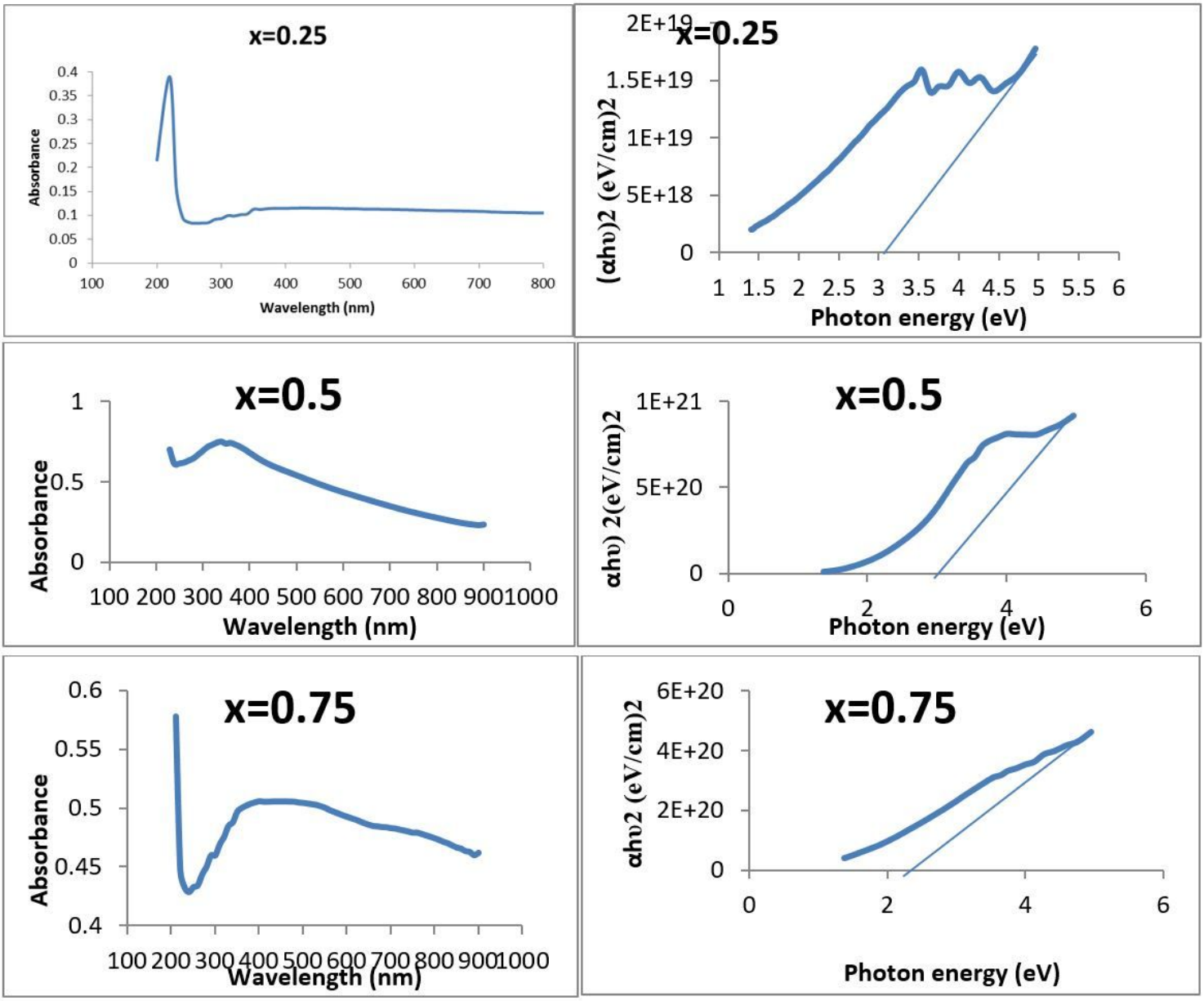

Figure 2

Electronic spectra and band gap of (a), 0.25, (b) 0.5 and (c) 0.75

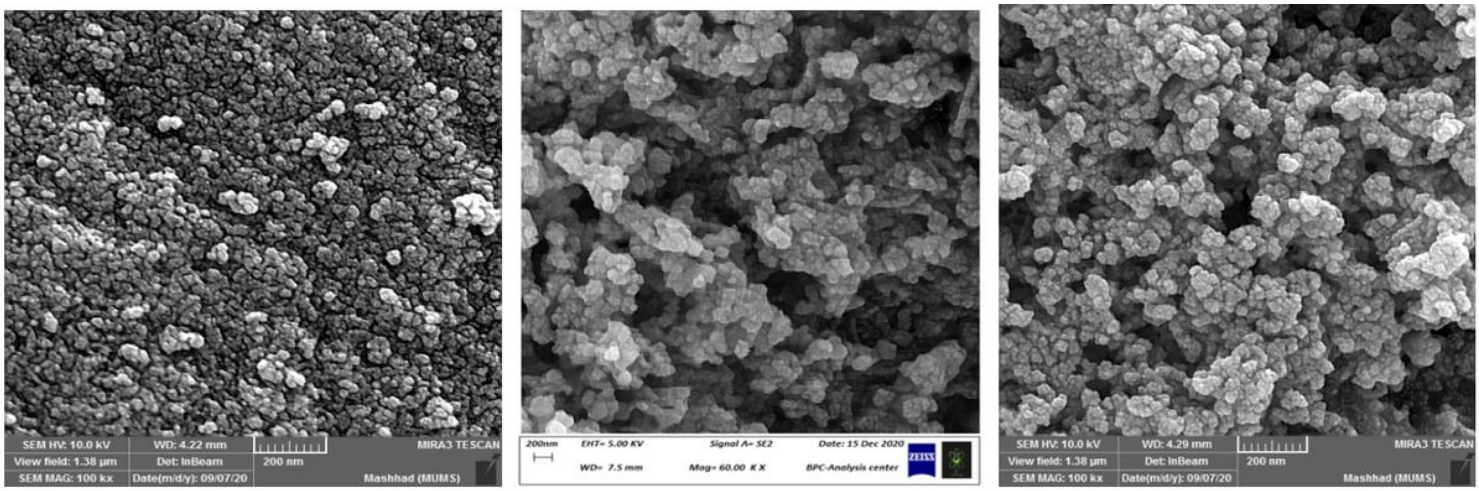

Figure 3

SEM of (a), 0.25, (b) 0.5 and (c) 0.75

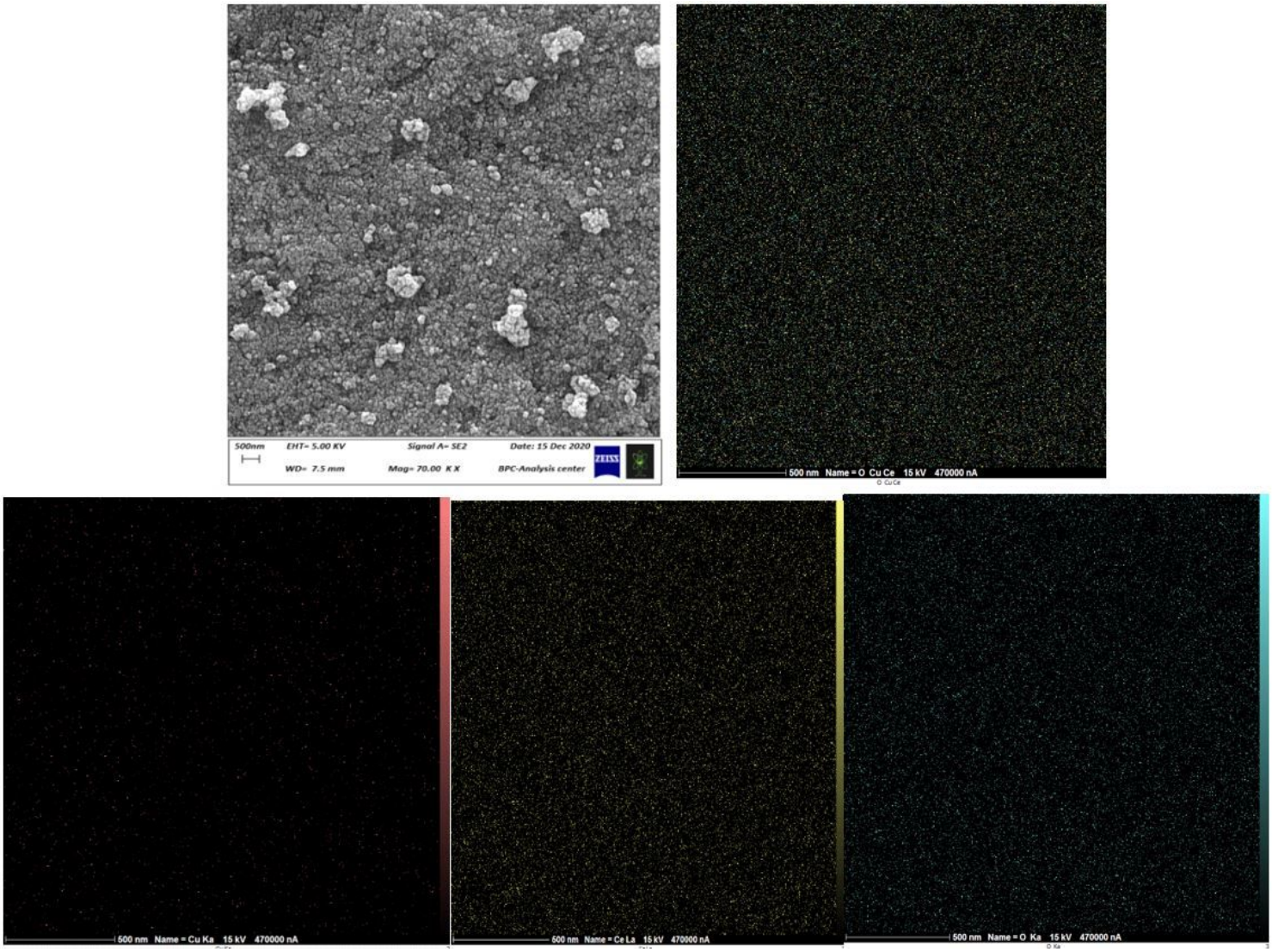

Figure 4

EDX mapping of CeO-CuO nanocomposite

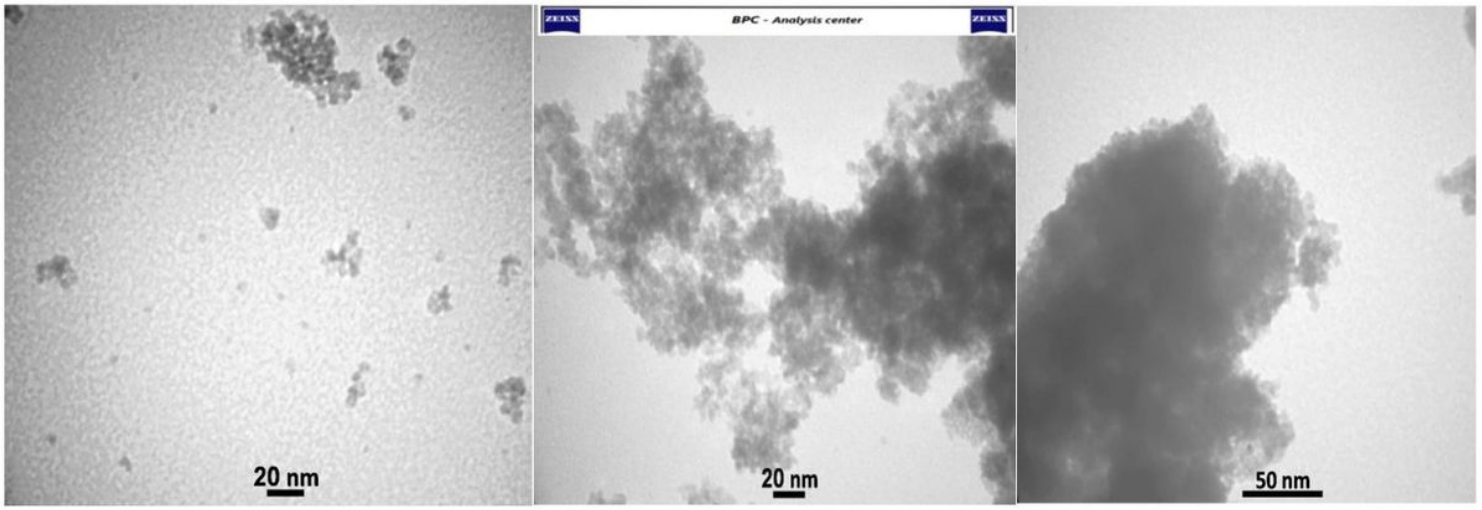

Figure 5

TEM of (a), 0.25, (b) 0.5 and (c) 0.75

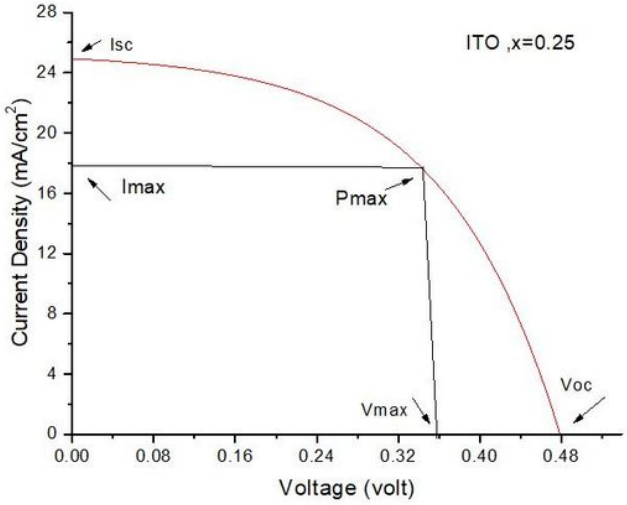

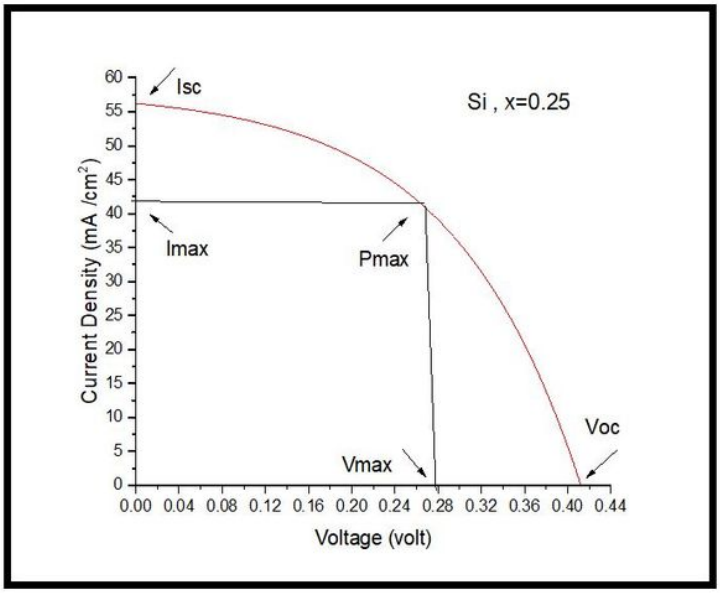

Figure 6

J-V characteristic for different types (ITO, Si) of electrode for (CuO)x–(CeO2)1-x, x=0.25

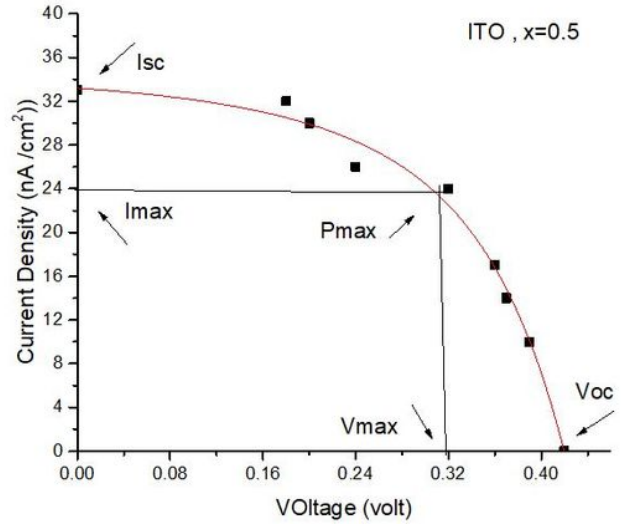

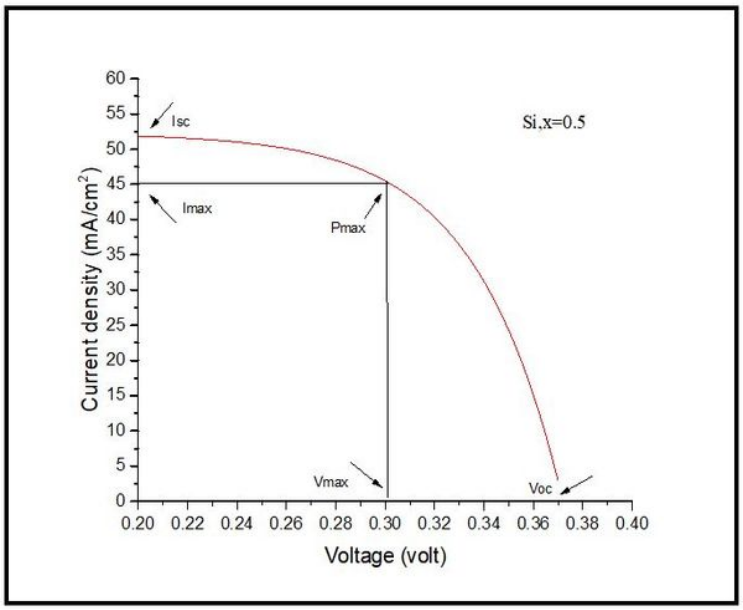

Figure 7

J-V characteristic for different types (ITO, Si) of electrode for (CuO)x–(CeO2)1-x, x=0.5

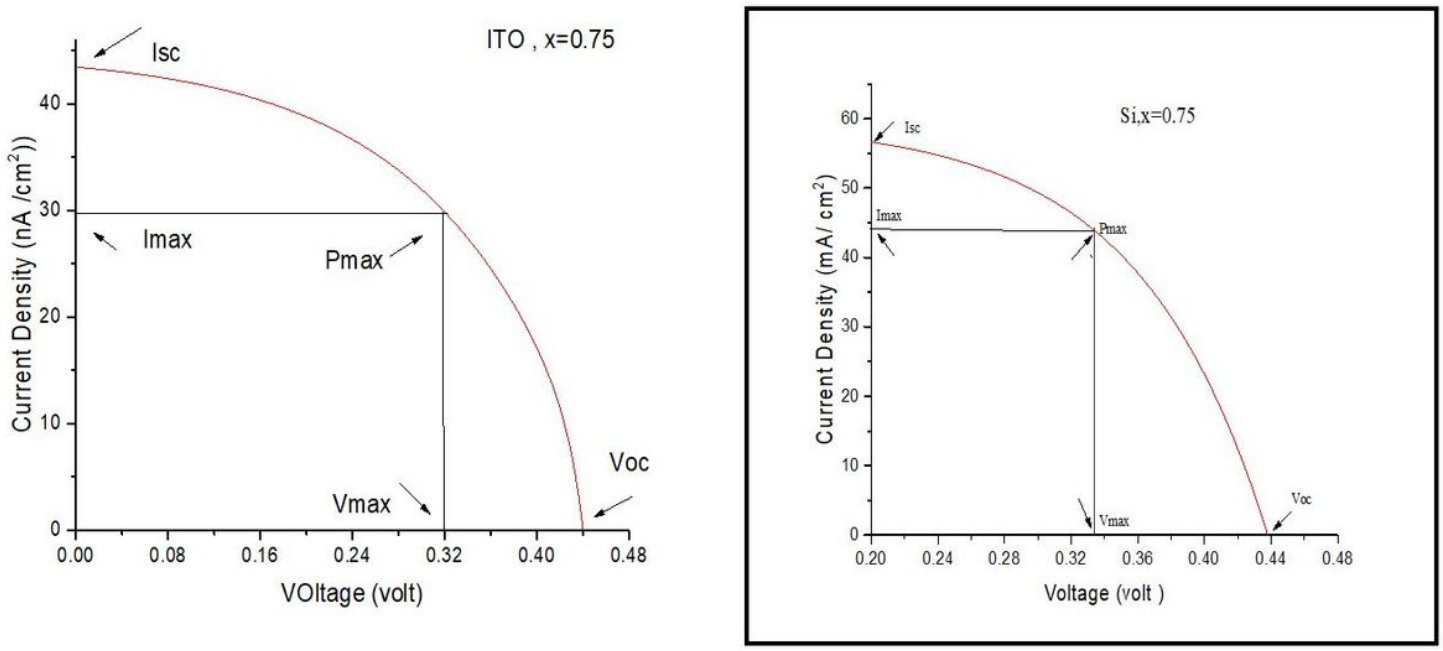

Figure 8

J-V characteristic for different types (ITO, Si) of electrode for (CuO)x–(CeO2)1-x, x=0.75